HiSST: 3rd International Conference on
High-Speed Vehicle Science Technology
14 -19 April 2024, Busan, Korea

Vibrational non-equilibrium effects in compressed and expanding hypersonic high enthalpy flow

Jan Martinez Schramm[1], Georgii Oblapenko[2]

Abstract

Atmospheric entry capsules shaped as spherically blunted, large apex-angle cones are widely used in space missions. Measurements in a hypersonic wind tunnel and numerical simulations on these types of capsules are performed. The comparing of the results of the experiments to the numerical simulation with respect to shock standoff distance and total drag allow for validation of the implemented physico-chemical models and the chemical relaxation rates in the numerical codes. The numerical reconstruction of the flow heavily depends on the accuracy of the assumed free stream used as an inflow conditions within the numerical simulations. The free stream of the wind tunnel experiments used as the inflow is obtained from numerical simulations of the hypersonic wind tunnel nozzle; here, the experimentally determined reservoir conditions of the wind tunnel nozzle determine the accuracy of the numerically determined freestream. Summarized we can state, that the measurements of the wind tunnel reservoir conditions drive the quality of the above mentioned validation process. The paper will present the work invested into determine the uncertainties of the validation process.

Keywords: hypersonic flow, *shock tunnel experiments, uncertainty quantification, thermochemical non-equilibrium, High Enthalpy Shock Tunnel Göttingen, HEG, numerical modelling, TAU*

Nomenclature

α_c – uncertain parameter governing chemical reaction rates
ρ – flow density
p_r – reservoir pressure
C_D – drag coefficient
F_D – drag force
S_k – first-order Sobol index
$S_{T,k}$ – total-order Sobol index
Ma – Mach number
u – free-stream velocity
h – specific enthalpy
Δ – shock standoff distance
F_x – force
θ – cone angle

1. Introduction

The experiments presented in this paper have been performed in the High Enthalpy Shock Tunnel (HEG). The HEG is a large-scale facility of the German Aerospace Center (DLR) and it is operated by the Department Spacecraft of the Institute of Aerodynamics and Flow Technology in Göttingen. The experimental investigations presented in this paper are focusing on a free stream Mach number of Ma = 7.4 at a flow speed of u = 2.4 km/s which corresponds to a total specific enthalpy of h = 3.2 MJ/kg of the test gas air. Experiments using the free flight model technique are performed. Free flying means that the models are not restricted in their movement during the hypersonic testing in any way. Shock shapes and acting forces on the models can be inferred during the experiments with

[1] *German Aerospace Center (DLR), Bunsenstraße 10, 37073 Göttingen, Germany, jan.martinez@dlr.de*
[2] *RWTH Aachen, Schinkelstraße 2, 52062 Aachen, Germany, georgii.oblapenko@rwth-aachen.de*

high precision. The work on hypersonic flow over spherically blunted cone capsules in air has been conducted and published in [6] and [7]. The experimental obtained data for the spherically blunted cone capsules, namely the shock standoff distance and the total drag, was compared to numerical simulations. The free stream data used for the numerical simulation is based on the numerical simulation of the wind tunnel nozzle. The nozzle computation uses the measured quantities of the reservoir condition as an input. The resulting free stream values have been used as a boundary input to numerically model the flow around the spherically blunted cone capsules and the results for shock standoff distance Δ and total force F_x in dependence of the cone angle θ have been compared to the experimental results for these quantities. As this work has already been published, only the most important results are briefly summarized here and the work is not discussed in detail. The focus of this publication will be the description of the numerical quantification of uncertainties in the numerical determination of the above-mentioned quantities shock standoff distance Δ and total Force F_x.

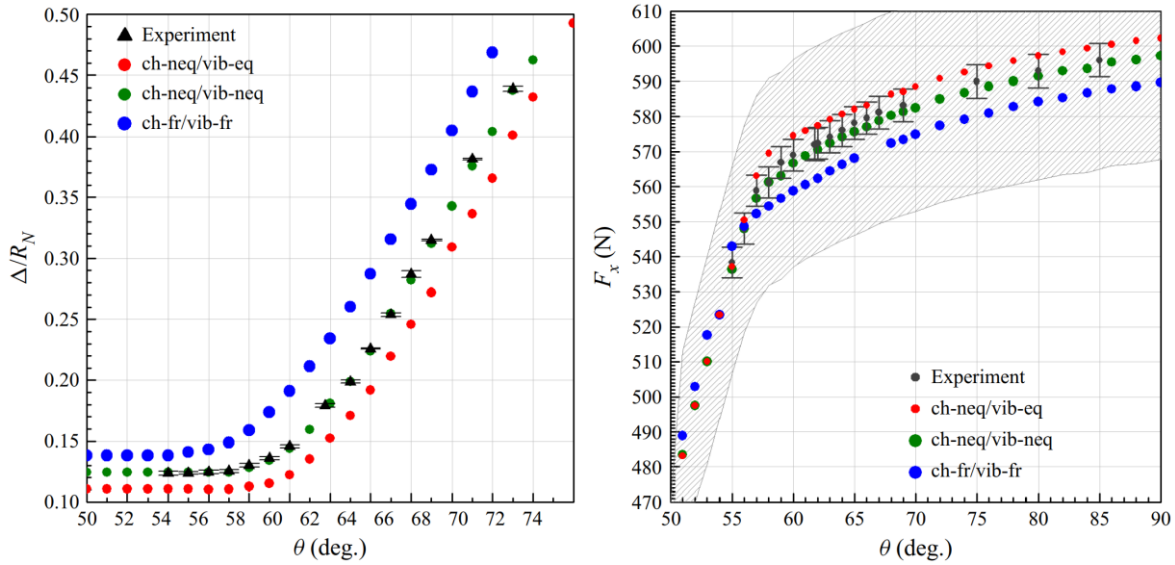

Fig 1. Measured and computed values of Δ/R_N plotted against θ, for a model with R^N = 24 mm. The computed values show results obtained with different physico-chemical models: chemical non-equilibrium and vibrational equilibrium (ch-neq/t-eq); chemical and vibrational non-equilibrium (ch-neq/t-neq); and frozen flow (ch-fr/t-fr). Mean value of ρu^2 for different sets of uncertain model parameters considered. Measured and computed values of the streamwise force component F_x plotted against θ for the models. The shaded region indicates the uncertainty in the computed force resulting from the free stream uncertainties.

Two results taken from [6] and [7] are shown in Fig 1. The experimentally determined shock standoff distance Δ as a function of the cone angle θ is shown on the left of Fig 1. The experimentally determined values for are shown with their corresponding accuracy, additionally the experimental results for different modelling approaches are shown. It can be clearly seen that the numerical simulation results assuming chemical non-equilibrium and vibrational non-equilibrium reproduce the experimental data best. The experimentally obtained forces F_x as a function of the cone angle θ are shown on the right of Fig 1, again the experimental obtained forces are plotted with their corresponding accuracy. Comparing the individual experimental results to the numerically reconstructed data it becomes evident, that the numerical results assuming chemical non-equilibrium and vibrational non-equilibrium reproduce the experimental results best. However, since the numerical data is based on the experimentally determined reservoir data of the hypersonic wind tunnel nozzle, the uncertainty of the numerical results was determined by repeated numerical calculation assuming the minimal and maximal bounds of the experimental reservoir data, e.g including the experimental uncertainty. The uncertainty is given as the shaded region in the right plot of Fig 1 and it is obvious that all differences in the numerical modelling assuming different chemical and vibrational modelling fall within this region. The question that arises is now if we can use the high precision experimental data and the numerical toolset to obtain a better estimation of the uncertainty of the measurements of the nozzle reservoir. In order to do so, we describe a polynomial chaos expansion approach used to infer a quantification of the

uncertainties in the numerical modelling process. Here, we vary the reservoir conditions and investigate the impact of the different physio-chemical modelling on the uncertainties.

2. Overview of numerical methodology

Numerical quantification of uncertainties in the forces acting on the blunted cones and analysis of the impact of uncertainties in reservoir parameters and chemical relaxation rates on the aforementioned uncertainties in the forces is performed using the Polynomial Chaos Expansion approach [1].

We assume that our quantity of interest Y (e.g. temperature, density, dynamic pressure, etc.) is dependent on some model parameters (e.g. reservoir pressure and temperature, chemical reaction rates; denoted by a vector $\boldsymbol{X}$) that have uncertainties associated with them. In order to evaluate the impact of these uncertainties on the uncertainty in Y, we expand Y into the following polynomial ansatz:

$$Y = \sum_{i=1}^{N} c_i \, \Phi_i(\boldsymbol{X}).$$

Here N is the polynomial degree, c_i are the unknown coefficients, and $\Phi_i(\boldsymbol{X})$ are predetermined polynomials of degree i of the uncertain model parameters. In the present work, we assume all uncertain model parameters to be uniformly distributed, and as such, choose the polynomials as Legendre polynomials. In the present work, the expansion coefficients c_i are obtained by evaluating the quantity of interest at $M > N$ different values of $\boldsymbol{X}$ and then solving the following overdetermined linear system:

$$\sum_{i=1}^{N} c_i \Phi(X_j) = Y(X_j), \; j = 1, \dots, M.$$

Having obtained the values of c_i, we can compute various statistical properties of our quantity of interest, such as the mean value $\overline{Y}$, standard deviation $\sigma(Y)$, and its sensitivity on the different uncertain model parameters. To this extent, we consider Sobol sensitivity indices, which describe the sensitivity of the quantity of interest with respect to the different uncertainties in the model parameters $\boldsymbol{X}$. The first-order indices are defined as

$$S_k = \frac{Var_k(E_{\sim k}(Y|X_k))}{\sigma^2(Y)},$$

and the total-order indices as

$$S_{T,k} = 1 - \frac{Var_{\sim k}(E_k(Y|\boldsymbol{X}_{\sim k}))}{\sigma^2(Y)}.$$

Here E and Var denote the computation of the expectation and variance, correspondingly. X_k is the k-th uncertain model parameter, $E_{\sim k}(Y|X_k)$ is the conditional expectation of the model over all uncertain model parameters except X_k; $(E_k(Y|\boldsymbol{X}_{\sim k})$ is the condition expectation of the model over only the model parameter X_k. Var_k is the variance computed over only X_k, and $Var_{\sim k}$ is the variance computed over all model parameters except X_k. Thus, the first-order Sobol index S_k quantifies the effect of varying only the model parameter X_k, averaging out the uncertainty due to the other parameters. In contrast, $S_{T,k}$ accounts for all higher-order interactions between parameter X_k and all other model parameters.

Depending on the number of uncertain model parameters considered, a large number of simulations may need to be carried out to provide sufficient statistics for accurate estimation of the expansion coefficients c_i. Therefore, the numerical analysis was split into two parts. First, quasi 1-D simulations were carried out for the flow inside the nozzle using the nozzle geometry data, but neglecting the influence of the turbulent boundary layer on the thickness of the core flow. As in this case the flow equations can be reduced to a set of ordinary differential equations, each such simulation can be carried out extremely fast; the full set of these quasi 1-D simulations can be then used to reduce the parameter space by assessing what impact different uncertain model parameters have on the flow physics [2]. As in this simplified setup the flow over the blunted cone is not computed, the value of the ρu^2 at the nozzle exit was used as a quantity of interest, as it directly related to the drag force acting on the blunted cone (if effects of thermochemical relaxation are neglected). Three different sets of simulations were considered: 1) with uncertainties in the reservoir pressure, reservoir temperature, exchange reaction rates, and dissociation reaction rates (in this case, the uncertainties in all the chemical reaction rates are described by two independent parameters), 2) with uncertainties in the reservoir pressure, reservoir temperature, and chemical reaction rates (in this case, one single uncertain parameter governs all reaction rates simultaneously), 3) with uncertainties in the reservoir pressure and chemical

reaction rates (variations in reservoir temperature are neglected).

After reducing the parameter space and assessing how many simulations need to be carried out for convergence, 2-D simulations were carried out using the DLR TAU CFD code [3]. The simulations were carried out on a 60x60 shock-fitted structured grid for 4 different cone nose half-angles (55°, 60°, 75°, 90°) with a shoulder radius of 4 mm and nose radius of 24 mm.

The reservoir pressure was assumed to have a mean value of 182.3 bar and an uncertainty of ±5%, the reservoir temperature was assumed to have a mean value of 2742 K and an uncertainty of ±0.29%. Standard 5-species air was used for the simulations, with 17 chemical reactions (15 dissociation and 2 Zeldovich exchange reactions). The chemical reaction rates were computed using the Arrhenius expression:

$$k_r(T) = A_r T^{n_r} exp(-\frac{E_{a,r}}{kT}),$$

with the pre-exponential factor A_r containing the model uncertainty:

$$log_{10} A_r = log_{10} A_{r,0} + \sigma_r \alpha_c.$$

Here α_c is the uncertain parameter (assumed in the present work to have a normal distribution with zero mean and a standard deviation of 1), and σ_r is a reaction-specific constant which governs how strongly that specific reaction rate coefficient is affected by the uncertain parameter. Typical values of σ_r are on the order of 0.1-0.15, and in the present work were based upon the values used in [4]. In case of two independent parameters governing the reaction rate uncertainties, α_D and α_E are used in place of α_c (corresponding to dissociation and exchange reactions, respectively).

3. 1-D simulation results

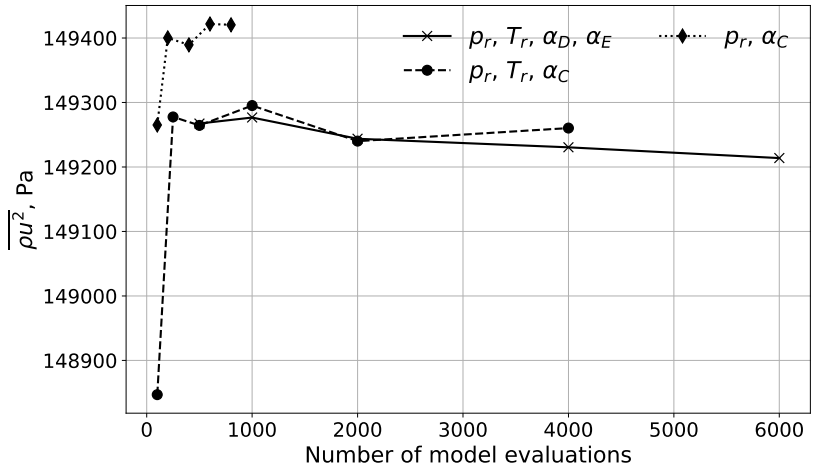

Fig 2. Mean value of ρu^2 for different sets of uncertain model parameters considered.

The mean value of ρu^2 at the nozzle exit for the three different sets of uncertain model parameters considered in the 1-D simulation is shown on Fig 2 as a function of the number of model evaluations. It can be seen that using a single parameter to describe uncertainties in the chemical reaction rates has very little impact on the mean value of ρu^2 at the nozzle exit. Neglecting variations in the reservoir temperature leads to slightly higher values of ρu^2, but the relative difference is approximately 0.1%, which is smaller than the experimental uncertainty.

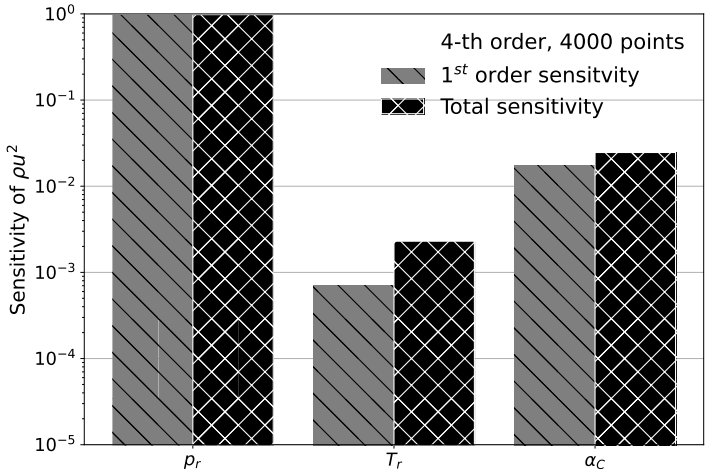

Fig 3. First- and total-order sensitivity indices of ρu^2 for the three-parameter simulation.

The sensitivity indices of ρu^2 at the nozzle exit are shown in Fig 3 for the simulation with three uncertain parameters. It can be seen that the uncertainty in the reservoir pressure has a much larger (approximately 2 orders of magnitude) impact on the uncertainty in ρu^2 compared to the uncertainties in the reservoir temperature and chemical reaction rates.

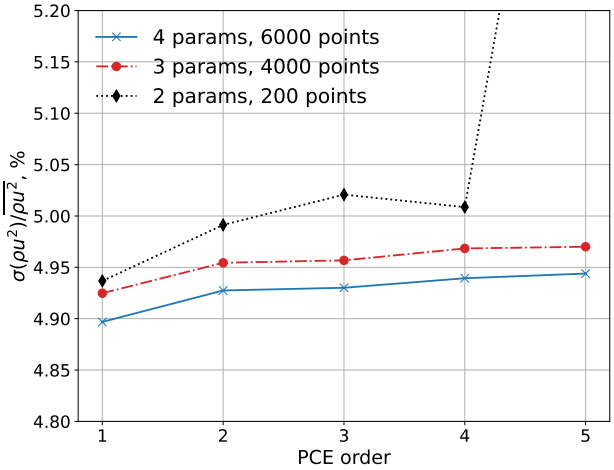

Fig 4. Relative uncertainties in ρu^2 for the different simulations.

Finally, the relative uncertainties in ρu^2 at the nozzle exit are shown on Fig 4 for the three different parameter sets considered in the 1-D simulations as a function of the PCE polynomial order. It can be seen that the two-parameter simulations slightly overestimate the uncertainty compared to the simulations with more uncertain parameters, but the difference is small, on the order of 0.05%. Moreover, with only 200 solutions and a 4-th order expansion, it is possible to get a good estimate of the uncertainty in ρu^2 (at higher expansion orders, more simulations are required, as otherwise the polynomial expansion overfits the data which leads to divergence of computed statistical properties).

Concluding the analysis based on the 1-D modelling, for the 2-D simulations it is sufficient to consider just two uncertain parameters (reservoir pressure and a single parameter for all the chemical reaction rates), as the difference with more detailed models is extremely small. This allows to perform relatively few 2-D simulations, significantly reducing the computational time required.

4. 2-D simulation results

Based on the results of the 1-dimensional analysis presented in the previous section, a simplified 2-dimensional model with only two uncertain parameters (reservoir pressure and a single parameter for all the chemical reaction rates) was considered. The modelling approach was divided into two parts. First, for each value of the reservoir pressure p_r and the parameter α_c governing the chemical reaction rates, a 2-dimensional axisymmetric simulation of the full HEG nozzle V was performed, assuming a

fully turbulent boundary layer and thermal equilibrium in the flow [5]. Due to the relatively low enthalpies of the flow, only 5-species air was considered, as the degree of ionization in the flow is negligible. Then the flow properties at the end of the nozzle were extracted from the simulation results and used as inflow boundary values for the subsequent simulations of the flow around the blunted cones, with each simulation using the corresponding value of α_c and accounting for thermal non-equilibrium effects. 280 simulations were carried out for each geometry. The geometries differed in the cone nose half-angles: 55°, 60°, 75°, 90°; all cones had a shoulder radius of 4 mm and nose radius of 24 mm. The simulations were performed on a 60x60 structured shock-fitted grid, as this was found to provide a good balance between simulation speed and numerical accuracy.

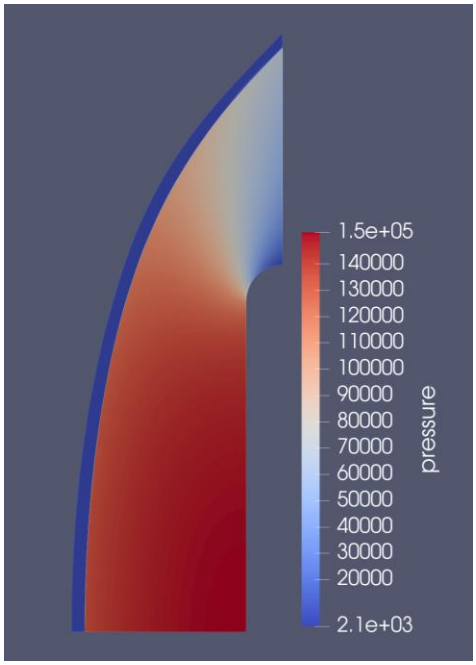

Fig 5. Example of computed flow-field, 90° cone half-angle. The flow quantity plotted is the pressure distribution around the model.

An example of a computed flow-field around the blunted cone is given on Fig 5 for the case of the 90° half-angle. From the simulations of the flow around the cones the drag forces and drag coefficients were computed and used in conjunction with the corresponding values of the reservoir pressure p_r and the parameter α_c to perform the analysis of the uncertainties and sensitivities.

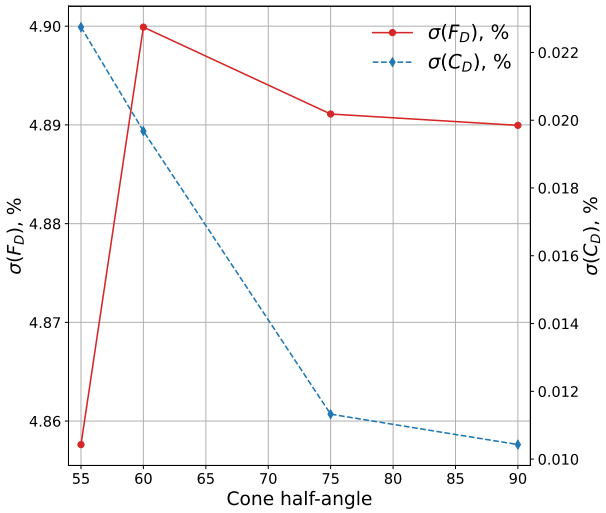

Fig 6. Uncertainties in the drag force and coefficient for different cone geometries.

Fig 6 shows the computed relative uncertainties in the drag force F_D and drag coefficient C_D for the different cone half-angles considered. It can be seen that the uncertainty in the drag force is on the

order of 5% (similar to the assumed uncertainty in the reservoir pressure) and does not vary strongly with the cone geometry. In contrast, the uncertainty in the drag coefficient decreases significantly with increasing cone half-angle; however, the overall uncertainty in the drag coefficient is extremely small, not exceeding 0.02%. Thus, the uncertainty in the drag force can be presumed to be mostly due to the uncertainty in the free-stream density and/or velocity, and not due to changes in the drag coefficient due to variations in the thermochemical relaxation rates.

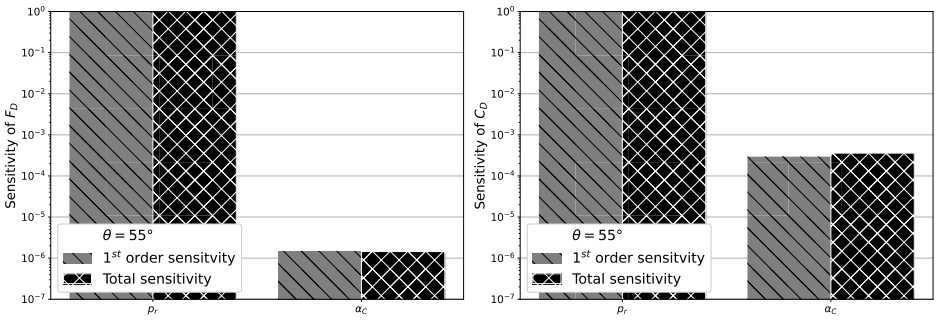

Fig 7. First- and total-order Sobol indices S_k and $S_{T,k}$ for the drag force (left) and drag coefficient (right), 55° half-angle.

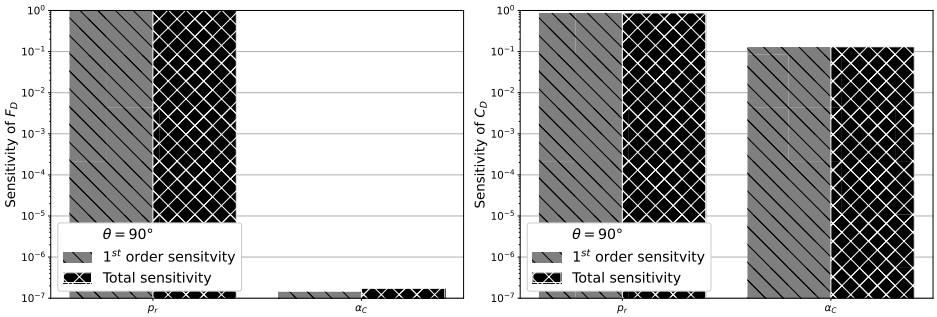

Fig 8. First- and total-order Sobol indices S_k and $S_{T,k}$ for the drag force (left) and drag coefficient (right), 90° half-angle.

Fig 7 to Fig 8 show the first- and total-order Sobol indices for the drag force (left) and coefficient (right) with respect to the different uncertain model parameters for two different cone geometries. We see that the impact of uncertainty in the chemical reaction rates (as described by α_c) on the uncertainty in the drag force is negligibly small compared to the impact of the uncertainty in the reservoir pressure. Chemical reaction rate uncertainty plays a larger role in the uncertainty in the drag coefficient (as seen in the right subplots), and the impact of this uncertainty increases with increasing cone half-angle. It is also worth noting that both for the drag force and drag coefficient, the first- and total-order sensitivity indices are almost identical, meaning that the uncertain parameters considered in the present work mostly have a direct first-order effect on the quantities of interest, and their higher-order interactions play almost no role.

Finally, we consider the question of inference of the actual reservoir pressure from the measured drag force, as the latter has been shown to have a significantly smaller measurements uncertainty compared to the reservoir pressure. Whilst in principle this can be done via Bayesian inference [4], potentially leveraging the PCEs obtained in the present work (as Bayesian inference requires a large number of simulation results to converge, and therefore benefits greatly from accurate reduced order models), from Fig 7 to Fig 8 we see that the sensitivity of the drag force with respect to the uncertainty in the reservoir pressure is well described the first-order Sobol index. That is, non-linear coupling effects between the different uncertain parameters have little impact on the drag force uncertainty. Thus, it is reasonable to first attempt using linear regression to model the dependence of the drag force on the reservoir pressure (neglecting the impact of uncertainties in the chemical reaction rates, as their impact can be seen to be very small). Since the model is linear, no complex inference approach would be required to deduce the actual reservoir pressure observed in the experiment from the measured drag force value: only a single linear equation needs to be solved.

Therefore, two linear regression models were fitted (one for the drag force F_D and one for the drag

coefficient C_D): $F_D = \zeta_D p_r + \eta_D$, $C_D = \zeta_C p_r + \eta_C$.

θ [°]	ζ_D	η_D	ζ_C	η_C.
55.00	28.08	15.19	0.0	8.56
60.00	30.06	11.33	0.0	9.01
75.00	31.2	12.83	0.0	9.37
90.00	31.67	13.16	0.0	9.53

Table 1. Linear regression fit coefficients for the different model nose half-angles.

Table 1 shows the linear regression fit coefficients for the different geometries considered in the simulations. The coefficients were rounded to two decimal points; therefore, due to the very small variations in the drag coefficient at lower cone half-angle values, the value of ζ_C is virtually zero.

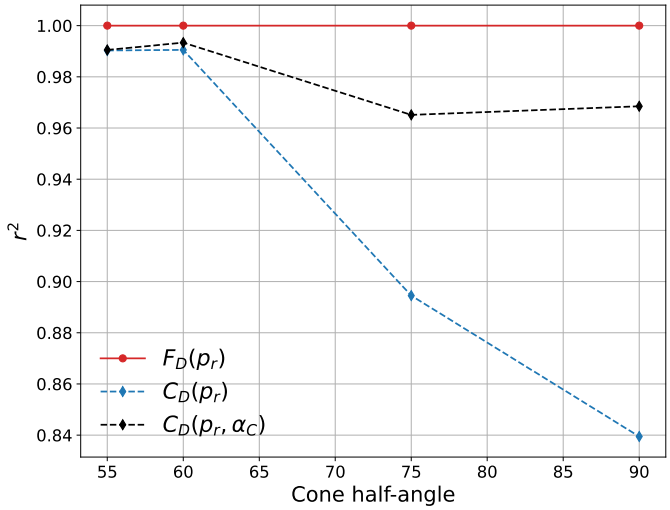

Fig 9. Coefficient of determination for the linear regression fits of the drag force and drag coefficient for the different cone half-angles.

The coefficient of determination (r^2) was computed to quantify the quality of the fit. Fig 9 shows the computed coefficient of determination as a function of the cone half-angle. It can be seen that the linear regression model provides an excellent description of the dependence of the drag force on the reservoir pressure and can indeed be used to infer the reservoir pressure from drag force measurements. The linear model has more error when used to predict the drag coefficient at higher half-angles, as the relaxation zone is larger, and chemistry plays a more important role. However, as seen previously, the actual variations in the drag coefficients are very small (and therefore, this impact of chemistry is much smaller compared to the impact of variations in the free-stream pressure due to the variations in the reservoir pressure when the drag force is considered). The third line on Fig 9 shows a two-parameter linear fit for the drag coefficient, incorporating the parameter α_c describing the variations in the chemical reaction rates. It can be seen that this improves the quality of the fit for the drag coefficient at higher cone half-angles.

The derived linear fit for the drag force in dependence on pressure is not geometry-independent, since it also includes the impact of the drag coefficient (the cross-sectional area of the models does not vary across different cone half-angles), which can also be seen from Table 1. However, since the variations in the drag coefficient have been shown to be negligibly small, a geometry-independent fit can be produced: $F_D/C_D = \widehat{\zeta_D} p_r + \widehat{\eta_D}$. For this final geometry-independent fit the values of the linear regression coefficients were found to be: $\widehat{\eta_D}$=1.4439, $\widehat{\zeta_D}$=3.3128. The r^2 of this fit for the different geometries was virtually 1.

5. Results

In Table 2 we list the experimentally determined forces acting on the different models (varying cone angle θ) with their corresponding accuracies. We can, with the help of the linear dependence formulation found above, infer the acting pressure in the wind tunnel nozzle reservoir for the individual experiments. The total average of the reservoir pressure found for the experiments is 184.72±0.87 bar, which gives us a precision of 0.5%. This is an order of magnitude lower than the precision we obtain by the pure experimental pressure measurements in the nozzle itself. The shot to shot variation in HEG for the reservoir pressure measurement is typically in the order of 1.5% while the precision considering the precision of the pressure transducers manufacturers rating is in the order of 5%. This combination leads to an uncertainty which drives the numerical free stream reconstruction and thus determines the error span given in Fig 1.

θ [°]	F_x[N]	σF_x[N]	p_r [bar]	σ p_r [bar]
57.00	558.80	4.470	184.644	1.512
58.00	561.20	4.490	184.644	1.512
59.00	566.90	4.535	184.644	1.512
60.00	569.00	4.552	185.496	1.519
61.75	572.00	4.576	184.644	1.512
62.00	572.40	4.579	184.644	1.512
63.00	574.20	4.594	184.644	1.512
64.00	576.10	4.609	184.644	1.512
65.00	578.20	4.626	184.644	1.512
66.00	579.60	4.637	184.644	1.512
67.00	581.20	4.650	184.644	1.512
69.00	583.20	4.666	184.644	1.512
75.00	590.00	4.720	184.978	1.515
80.00	593.00	4.744	184.644	1.512
85.00	596.00	4.760	184.644	1.509
			184.72	**0.87**

Table 2. Reversely determined reservoir pressures of the wind tunnel experiments based on the experimental measurements of the acting forces on the free flying wind tunnel models.

6. Conclusion

The underlying idea for this publication was to use absolute highly accurate and precise force measurements on free-flying models in a hypersonic wind tunnel to improve the determination of the uncertainty of pressure measurements in the reservoir region of HEG´s wind tunnel nozzle. Published experimental and numerical work on forces measurements on large apex-angle cones were shortly presented and an error analysis based on the polynomial chaos expansion approach was performed. It could be shown that the uncertainty imposed by chemical reaction rates on the uncertainty of the drag force is negligibly small compared to the impact of the uncertainty in the reservoir pressure. A linear regression describes the dependence of drag force uncertainty on the reservoir pressure uncertainty perfectly. This in turn means, that the pressure instrumentation having typically an uncertainty of 5% (resulting mainly from the low precision of the sensor itself) shows a much better accuracy (a priori unknown) than expected.

7. Acknowledgments

Georgii Oblapenko acknowledges the funding provided by the Alexander von Humboldt foundation for his stay as a guest researcher at the German Aerospace Center (DLR), during which this work was carried out.

References

1. Smith, R.: Uncertainty Quantification: Theory, Implementation, and Applications. SIAM, Philadelphia (2014)
2. Oblapenko, G., Hannemann, V.: Sensitivity Analysis of Non-equilibrium Expanding High-Enthalpy Flows, AIAA Scitech (2023). https://doi.org/10.2514/6.2023-1139

3. Mack, A., Hannemann, V.: Validation of the Unstructured DLR-TAU-Code for Hypersonic Flows, 32nd AIAA Fluid Dynamics Conference and Exhibit (2002). https://doi.org/10.2514/6.2002-3111
4. Cortesi, A.F., Constantine, P.G., Magin, T.E., Congedo, P.M.: Forward and backward uncertainty quantification with active subspaces: application to hypersonic flows around a cylinder, J. Comp. Phys. (2020). https://doi.org/10.1016/j.jcp.2019.109079
5. Hannemann, K., Martinez Schramm, J., Wagner, A., Ponchio Camillo, G.: The High Enthalpy Shock Tunnel Göttingen of the German Aerospace Center (DLR), Journal of Large-Scale Research Facilities JLSRF (2018). https://doi.org/10.17815/jslrf-4-168
6. Hornung, H. G., Martinez Schramm, J. & Hannemann, K.: Hypersonic flow over spherically blunted cone capsules for atmospheric entry. Part 1. the sharp cone and the sphere. Journal of Fluid Mechanics 871, 1097 – 1116 (2019)
7. Martinez Schramm, J., Hannemann, K., & Hornung, H.: Hypersonic flow over spherically blunted cone capsules for atmospheric entry. Part 2. Vibrational non-equilibrium effects. Journal of Fluid Mechanics, 954, A32. doi:10.1017/jfm.2022.1014 (2023)